Non-Data-Aided Spectral-Line Method for Fine Carrier Frequency Synchronization in OFDM Receivers

Heejin Roh and Kyungwhoon Cheun

Abstract: **A nonlinear spectral-line method utilizing the fourth absolute moment of the receiver discrete Fourier transform output is proposed as a non-data-aided fine carrier frequency synchronization algorithm for OFDM receivers. A simple modification of the algorithm resulting in low implementation complexity is also developed. Analytic expressions are derived for the steady-state frequency error variances of the algorithms and verified to be very accurate via computer simulations over AWGN and frequency selective multipath channels. Numerical results show that the proposed algorithms provide reliable and excellent steady-state performance, especially with PSK modulation. Also, the proposed algorithms are insensitive to symbol timing offsets, only requiring a coarse symbol timing recovery.**

Index Terms: **Frequency offset, interchannel interference, multipath channels, orthogonal frequency division multiplexing (OFDM), synchronization.**

I. INTRODUCTION

There has been increasing interest in orthogonal frequency division multiplexing (OFDM) modulation due to various advantages over single carrier systems such as immunity to impulsive noise and tolerance against frequency selective multipath distortion [1]. Due to these advantages, OFDM was adopted for broadcast transmission systems such as digital audio broadcasting (DAB) and terrestrial digital video broadcasting (DVB-T) [2]. Recently, the IEEE 802.11 standardization group also selected OFDM as the basis for the 2.4 and 5 GHz band physical layer standards for wireless local and metropolitan area networks [3], [4].

High sensitivity to carrier frequency offsets caused by Doppler shift and frequency mismatch between the transmitter and the receiver local oscillators is, however, a major drawback of OFDM systems [5]. In OFDM receivers, a carrier frequency offset of Δf_c may be decomposed into an integer multiple of the subcarrier spacing denoted f_d and a fractional frequency offset denoted δf_c, i.e., $\Delta f_c = \epsilon_I f_d + \delta f_c$ where ϵ_I is an integer and $-f_d/2 \leq \delta f_c < f_d/2$. The term $\epsilon_I f_d$ simply shifts the transmitted signal in the frequency domain by ϵ_I times the subcarrier spacing but the fractional carrier frequency offset δf_c not only results in a decrease in the desired signal power at the receiver discrete Fourier transform (DFT) output but also incurs interchannel interference (ICI), severely degrading the bit error rate performance of the receiver [5]–[7].

Many of the recent work on estimating the carrier frequency offset focus on the utilization of a training sequence and maximum-likelihood (ML) estimation. Moose in [6] proposed an algorithm for ML estimation of the carrier frequency offset assuming that a training symbol is transmitted in two consecutive OFDM symbols. Schmidl and Cox in [8] presented an ML algorithm exploiting the phase difference between the former and the latter halves of one known OFDM symbol with two identical halves. Morelli and Mengali in [9] modified the algorithm proposed by Schmidl and Cox to extend the frequency acquisition range at the cost of degraded steady-state performance.

On the other hand, non-data aided (NDA) approaches for carrier frequency synchronization have also been studied. Daffara and Adami in [7] proposed an algorithm exploiting the redundancy contained within the cyclic prefix. In [10], van de Beek *et al.* presented an ML estimation algorithm using the cyclic prefix for jointly estimating the carrier frequency and timing offsets. However, delay lines of length equal to the DFT length are required for the algorithms, resulting in high implementation complexity.

In this paper, we develop a simple NDA solution to compensate for carrier frequency offsets. We will show that the $2p$th absolute moments (p integer ≥ 1) of the receiver DFT outputs can be expressed in terms of a weighted sum of sinusoids. The sinusoids have frequencies that are integer multiples of the reciprocal of the subcarrier spacing evaluated at the fractional carrier frequency offset δf_c. Based on this argument, we propose and analyze an algorithm for fine carrier frequency synchronization utilizing the fourth absolute moment ($p = 2$) of the DFT outputs. The baseline algorithm is rather complex, requiring a secondary DFT processor but a simple modification allows us to do away with the additional DFT processor. The proposed algorithms will force the carrier frequency offset to the nearest integer multiple of the subcarrier spacing after which a secondary carrier recovery step is required to compensate for the residual carrier frequency offset of an integer multiple of the subcarrier spacing (see, e.g., [11]). We derive analytical expressions for steady-state frequency error variances of the proposed algorithms and verify their accuracy via computer simulation over AWGN and a frequency selective multipath channel given in [2] modeling an urban area.

The remainder of this paper is organized as follows. Section II describes the OFDM system considered in this paper and defines the related terminologies used in subsequent sections. The proposed carrier frequency synchronization algorithms are derived in Section III and analyzed in Section IV. The analytical results

Manuscript received February 7, 2003; approved for publication by Shigeaki Ogose, Division II Editor, December 25, 2003.

H. Roh is with Samsung Electronics Co., Ltd., Korea, email: hjroh71@hanmail.net.

K. Cheun is with the Division of Electrical and Computer Engineering, Pohang University of Science and Technology (POSTECH,) Pohang 790-784, Korea, email: cheun@postech.ac.kr.

This work was supported by grant R01-2003 from the Basic Research Program of the Korea Science & Engineering Foundation (KOSEF).

are then confirmed via computer simulations for QPSK and 64-QAM subcarrier modulations over AWGN and frequency selective multipath channels in Section V and finally, conclusions are drawn in Section VI.

II. SYSTEM MODEL

In the OFDM transmission system model under consideration, $(2M+1)$ data symbols are modulated onto $(2M+1)$ subcarriers termed the *active carriers* via an N-point ($N \geq 2M+1$) inverse DFT (IDFT). The remaining $(N-2M-1)$ subcarriers termed the *virtual carriers* are not assigned for data modulation and are equally placed on either side of the $(2M+1)$ active carriers. The frequency band occupied by one-sided virtual carriers is called a *guard band*. The N-point IDFT output sequence is called an *OFDM symbol* and each sample is referred to as an *OFDM sample*. A guard-interval, or *cyclic prefix*, containing a replica of the last N_g OFDM samples of the OFDM symbol is then inserted at the beginning of the OFDM symbol in order to avoid intersymbol interference (ISI). The complex baseband envelope of the transmitted OFDM signal is then modeled as [2]

$$x(t) = \frac{1}{\sqrt{N}} \sum_{m=-\infty}^{\infty} \sum_{k=-M}^{M} X_{k,m} \xi_k(t - mT). \quad (1)$$

Here, $X_{k,m}$ is the transmitted data symbol on the kth subcarrier of the mth OFDM symbol assumed to be statistically independent and identically distributed (i.i.d.), $T \triangleq (N_g+N)T_s$ with T_s denoting the OFDM sample period and $\xi_k(t)$ is given by

$$\xi_k(t) = \begin{cases} \exp(j2\pi k f_d t), & -N_g T_s \leq t < NT_s \\ 0, & \text{otherwise,} \end{cases} \quad (2)$$

where $f_d \triangleq 1/NT_s$ denotes the subcarrier spacing. The signal is then transmitted over a frequency selective multipath fading channel with I multipath components with equivalent lowpass impulse response

$$h(t) = \sum_{i=0}^{I-1} h_i \delta(t - \tau_i), \quad (3)$$

where τ_i and h_i are the delay and the complex path gain of the ith path, respectively. We assume that the channel is constant during intervals of T and $\tau_0 < \tau_1 < \cdots < \tau_{I-1} < N_g T_s$ with $\tau_0 = 0$.

To simplify our discussion, we assume that the receive filter is an ideal lowpass filter with a cut-off frequency equal to $1/2T_s$. We also assume that the magnitude of the initial carrier frequency offset is sufficiently less than the guard band so that the filtered received signal can be expressed as

$$y(t) = \sum_{i=0}^{I-1} h_i x(t - \tau_i) e^{j2\pi \Delta f_c t} + w(t), \quad (4)$$

where Δf_c is the carrier frequency offset and $w(t)$ is the response of the receive filter to a zero mean complex additive white Gaussian noise (AWGN).

Consider the demodulation of the mth OFDM symbol. Sampling $y(t)$ at time instants $t = mT + nT_s, n = 0, 1, \cdots, N-1$, yields the following N-point input sequence presented to the DFT block[1]

$$\begin{aligned} y_n &= \sum_{i=0}^{I-1} h_i x(mT + nT_s - \tau_i) e^{j2\pi\epsilon n/N + j\phi} + w_n \\ &= \frac{1}{\sqrt{N}} \sum_{l=-M}^{M} H_l X_l e^{j2\pi(l+\epsilon)n/N + j\phi} + w_n. \end{aligned} \quad (5)$$

Here, $H_l \triangleq \sum_{i=0}^{I-1} h_i \exp(-j2\pi l \tau_i f_d)$ is the frequency response of the channel at the lth subcarrier, $\epsilon \triangleq \Delta f_c / f_d$ is the normalized carrier frequency offset, $\phi \triangleq 2\pi m\epsilon(1 + N_g/N)$ and $w_n \triangleq w(mT + nT_s)$. The dependence of samples y_n, w_n, and X_l on m was dropped for notational simplicity. The kth DFT output denoted Y_k is then given by

$$\begin{aligned} Y_k &= \frac{1}{\sqrt{N}} \sum_{n=0}^{N-1} y_n e^{-j2\pi nk/N}, \\ & \qquad k = -N/2, -N/2+1, \cdots, N/2-1. \end{aligned} \quad (6)$$

Substituting (5) into (6) then yields

$$\begin{aligned} Y_k &= \sum_{l=-M}^{M} H_l X_l e^{j\phi} \Psi(l - k + \epsilon) + W_k, \\ & \qquad k = -N/2, -N/2+1, \cdots, N/2-1, \end{aligned} \quad (7)$$

where the kth DFT output of the noise samples $\{w_n\}_{n=0}^{N-1}$, denoted W_k, is a zero mean complex white Gaussian random variable with variance $\sigma_n^2 \triangleq E\{|W_k|^2\}$ and $\Psi(x)$ is defined as

$$\begin{aligned} \Psi(x) &\triangleq \frac{1}{N} \sum_{n=0}^{N-1} e^{j2\pi xn/N} \\ &= \sum_{m=-\infty}^{\infty} e^{j\pi(x+mN)(1-1/N)} \frac{\sin(\pi(x+mN))}{N \sin\left(\frac{\pi(x+mN)}{N}\right)}. \end{aligned} \quad (8)$$

Note that $\Psi(x) \simeq e^{j\pi x(1-1/N)} \mathrm{sinc}(x)$ for $|x|/N \ll 1$, where $\mathrm{sinc}(x) \triangleq \sin(\pi x)/(\pi x)$.

Recalling that $\Delta f_c = \epsilon_I f_d + \delta f_c$, we have $\epsilon = \epsilon_I + \epsilon_F$ with $\epsilon_F \triangleq \delta f_c / f_d$ $(-1/2 \leq \epsilon_F < 1/2)$ being the normalized fractional carrier frequency offset. From (7), Y_k can then be written as

$$Y_k = \begin{cases} H_{k-\epsilon_I} X_{k-\epsilon_I} e^{j\phi} \Psi(\epsilon_F) + V_k + W_k, \\ \qquad -M + \epsilon_I \leq k \leq M + \epsilon_I \\ V_k + W_k, \qquad \text{otherwise,} \end{cases} \quad (9)$$

where V_k denotes the ICI term due to ϵ_F given by

$$V_k = \sum_{\substack{l=-M \\ l \neq k-\epsilon_I}}^{M} H_l X_l e^{j\phi} \Psi(l - k + \epsilon). \quad (10)$$

[1]Though for the sake of mathematical simplicity, we assume perfect symbol timing recovery in the derivation of the algorithm, simulation results show that the algorithms exhibit very robust performance in the presence of symbol timing errors.

Note from (9) that the data symbol transmitted at the kth IDFT input, X_k, is received at the $(k+\epsilon_I)$th DFT output due to the integer carrier frequency offset component $\epsilon_I f_d$ and is weighted by $\Psi(\epsilon_F)$ which effectively decreases the received power of the desired data symbol.

III. THE ALGORITHM

A. Nonlinear Spectral-Line Frequency Synchronization

In this section, we describe the algorithm for estimating the fractional carrier frequency offset ϵ_F by observing the absolute moments of the receiver DFT outputs. Using a change of variable, the DFT output Y_k in (7) can be written as

$$Y_k = \sum_{l=-M+\epsilon_I}^{M+\epsilon_I} H_{l-\epsilon_I} X_{l-\epsilon_I} e^{j\phi} \Psi(l-k+\epsilon_F) + W_k, \quad k = -N/2, -N/2+1, \cdots, N/2-1. \tag{11}$$

Recall that $|\epsilon|$ is sufficiently less than ϵ_{GB} where $\epsilon_{GB} \triangleq N/2 - M - 1$ is the guard band normalized by the subcarrier spacing. Then, since $|\Psi(x)|$ behaves as $|\mathrm{sinc}(x)|$, we may safely assume that Y_k for $|k| \le M' \triangleq M - \epsilon_{GB}$ is insensitive to X_l for $|l| > M$. This allows us to extend the lower and upper limits of the summation in (11) to $-N/2$ and $N/2-1$, respectively, for the range of $|k| \le M'$. Hence, the $(2M'+1)$ DFT outputs can be expressed as

$$Y_k = \sum_{l=-N/2}^{N/2-1} H_{l-\epsilon_I} X_{l-\epsilon_I} e^{j\phi} \Psi_l^k + W_k, \quad k = -M', -M'+1, \cdots, M', \tag{12}$$

where Ψ_l^k is a shorthand for $\Psi(l-k+\epsilon_F)$. Since W_k is a zero mean Gaussian random variable uncorrelated with $H_{l-\epsilon_I}$'s and $X_{l-\epsilon_I}$'s, the $2p$th absolute moment of Y_k, namely $E\{|Y_k|^{2p}\}$ ($p \ge 1$, integer) for $|k| \le M'$ can easily be computed to be

$$E\{|Y_k|^{2p}\} = \sum_{q=0}^{p} \binom{p}{q} E\{|\tilde{Y}_k|^{2q}\} E\{|W_k|^{2p-2q}\}, \tag{13}$$

where $\tilde{Y}_k \triangleq Y_k - W_k$.

For the time being, let us assume a perfect channel and set $H_{l-\epsilon_I} = 1$ for all l. Then, it is shown in Appendix A that $E\{|Y_k|^{2q}\}$ is a linear combination of $\cos(2\pi m\epsilon_F)$, $m = 0, \pm1, \pm2, \cdots, \pm(q-1)$ and in turn, $E\{|Y_k|^{2p}\}$ of (13) is a linear combination of $\cos(2\pi m\epsilon_F)$, $m = 0, \pm1, \pm2, \cdots, \pm(p-1)$. Recalling that $\epsilon_F = \delta f_c / f_d$, $E\{|Y_k|^{2p}\}$ can thus be expressed as

$$E\{|Y_k|^{2p}\} = \sum_{m=-(p-1)}^{p-1} g_m \cos\left(2\pi \frac{m}{f_d} \delta f_c\right), \tag{14}$$

for some set of constants $\{g_m\}$. That is, the $2p$th absolute moment of the DFT output is a linear combination of sinusoids (spectral-lines) with frequencies that are integer multiples of $1/f_d$ evaluated at δf_c. For $p = 1$, however, $E\{|Y_k|^2\}$ reduces to a constant, giving no information about the fractional carrier frequency offset. Hence, we can only consider the case when $p \ge 2$. Note that this is very similar to the spectral-line method for symbol timing recovery in single carrier systems [13].

B. Scheme A: Case of $p = 2$

For this specific case, it is practically feasible to consider the effect of multipath interference. We assume that given a positive integer q, the $2q$th absolute moments of the channel responses in (12) are identically distributed for all subcarriers, i.e., $E\{|H_{l-\epsilon_I}|^{2q}\} = E\{|H_k|^{2q}\}$ for all l. Since $X_{l-\epsilon_I}$'s in (12) are assumed to be statistically i.i.d., substituting (12) into (13) with $p = 2$ and expanding the resulting expression yields

$$\begin{aligned} E\{|Y_k|^4\} &= E\{|H_k|^4\} E\{|X_k|^4\} \sum_{l=-N/2}^{N/2-1} |\Psi_l^k|^4 \\ &\quad + 2\left(E\{|X_k|^2\}\right)^2 \sum_{\substack{l_1=-N/2 \\ l_1 \ne l_2}}^{N/2-1} \sum_{l_2=-N/2}^{N/2-1} E\{|H_{l_1-\epsilon_I} H_{l_2-\epsilon_I}|^2\} \\ &\quad \times |\Psi_{l_1}^k|^2 |\Psi_{l_2}^k|^2 + E\{|W_k|^4\} + 2\sigma_s^2 E\{|W_k|^2\} \sum_{l=-N/2}^{N/2-1} |\Psi_l^k|^2 \\ &= -\rho_1 \sum_{l=-N/2}^{N/2-1} |\Psi_l^k|^4 + 2\left(E\{|X_k|^2\}\right)^2 \\ &\quad \times \sum_{l_1=-N/2}^{N/2-1} \sum_{l_2=-N/2}^{N/2-1} E\{|H_{l_1-\epsilon_I} H_{l_2-\epsilon_I}|^2\} |\Psi_{l_1}^k|^2 |\Psi_{l_2}^k|^2 \\ &\quad + E\{|W_k|^4\} + 2\sigma_s^2\sigma_n^2 \sum_{l=-N/2}^{N/2-1} |\Psi_l^k|^2, \end{aligned} \tag{15}$$

where $\rho_1 \triangleq E\{|H_k|^4\}\left(2\left(E\{|X_k|^2\}\right)^2 - E\{|X_k|^4\}\right)$ and $\sigma_s^2 \triangleq E\{|H_k|^2\} E\{|X_k|^2\}$. Note that the double summation in the second term of (15) is dominated by values of l_1 and l_2 that are closely spaced due to the fact that $|\Psi_{l_1}^k|^2 |\Psi_{l_2}^k|^2$ is inversely proportional to $(l_1 - k + \epsilon_F)^2 (l_2 - k + \epsilon_F)^2$. Assuming that the channel response is approximately constant among the closely spaced subcarriers, we may then approximate

$$\sum_{l_1=-N/2}^{N/2-1} \sum_{l_2=-N/2}^{N/2-1} E\{|H_{l_1-\epsilon_I} H_{l_2-\epsilon_I}|^2\} |\Psi_{l_1}^k|^2 |\Psi_{l_2}^k|^2 \simeq E\{|H_k|^4\} \left(\sum_{l=-N/2}^{N/2-1} |\Psi_l^k|^2\right)^2. \tag{16}$$

Hence, substituting (16) into (15) yields

$$E\{|Y_k|^4\} \simeq -\rho_1 \Gamma_2(\epsilon_F) + \rho_2 \Gamma_1^2(\epsilon_F) + 2\sigma_s^2\sigma_n^2 \Gamma_1(\epsilon_F) + E\{|W_k|^4\}, \tag{17}$$

where $\rho_2 \triangleq 2E\{|H_k|^4\}\left(E\{|X_k|^2\}\right)^2$ and $\Gamma_q(\epsilon_F)$ is defined as

$$\Gamma_q(\epsilon_F) \triangleq \sum_{l=-N/2}^{N/2-1} |\Psi_l^k|^{2q}. \tag{18}$$

Note from (B.48) that (17) can be written as $c_1 + c_2 \cos(2\pi\epsilon_F)$ with appropriate constants c_1 and c_2. By differentiating this with respect to ϵ_F, we can obtain a valid error signal for ϵ_F.

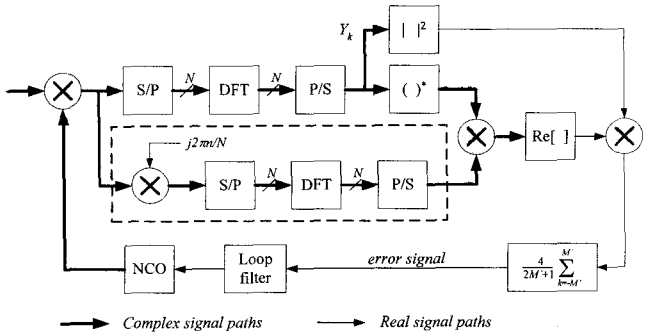

Fig. 1. Block diagram of the proposed frequency synchronization loop (Scheme A).

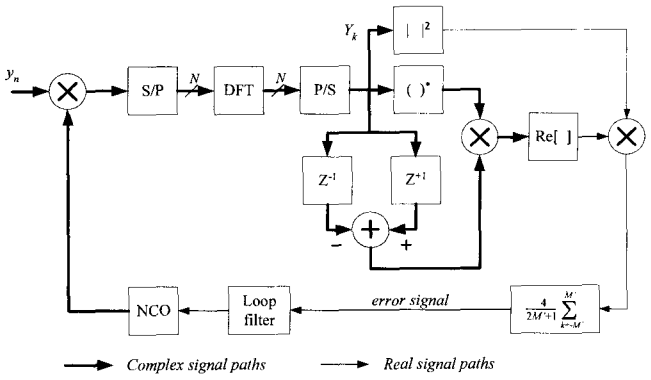

Fig. 2. Block diagram of the simplified frequency synchronization loop (Scheme B).

Since it is easily checked from (12) that Y_k for $|k| \leq M'$ have identical statistical properties, an estimate of $E\{|Y_k|^4\}$ is given by

$$m(\epsilon_F) = \frac{1}{2M'+1} \sum_{k=-M'}^{M'} |Y_k|^4. \quad (19)$$

Hence, a stochastic update error signal can be obtained by differentiating $m(\epsilon_F)$ with respect to ϵ_F, given as

$$e(\epsilon_F) \triangleq \frac{\partial}{\partial \epsilon_F} m(\epsilon_F) = \frac{4}{2M'+1} \sum_{k=-M'}^{M'} |Y_k|^2 \operatorname{Re}\left[Y_k^* \frac{\partial}{\partial \epsilon_F} Y_k\right], \quad (20)$$

where $\operatorname{Re}[x]$ denotes the real part of x. Also, it follows from (6) that $\partial Y_k/\partial \epsilon_F$ in (20) is given as

$$\frac{\partial}{\partial \epsilon_F} Y_k = \frac{1}{\sqrt{N}} \sum_{n=0}^{N-1} \left(j\frac{2\pi n}{N} y_n\right) e^{-j2\pi nk/N}. \quad (21)$$

Fig. 1 shows the block diagram of synchronization loop employing the proposed frequency error detector (FED) based on (20). Note that an additional DFT block indicated by the dashed box is required for computing $\partial Y_k/\partial \epsilon_F$, resulting in quite high implementation complexity. We refer to this algorithm as *Scheme A*.

C. Scheme B: Simplified Algorithm

Applying the interpolation formula [11, eq. (2-2-37), p. 73] yields the following approximated reconstruction for $Y(f)$

$$Y(f) \simeq \sum_{m=-M+\epsilon_I}^{M+\epsilon_I} Y_m \operatorname{sinc}(f/f_d - m - \epsilon_F). \quad (22)$$

By applying the discrete-time derivative technique [12, p. 760–761] to (22), we obtain

$$\frac{\partial}{\partial \epsilon_F} Y_k \simeq \left[\frac{\partial}{\partial f} Y(f)\right]_{f=(k+\epsilon_F)f_d} = \sum_{m=-M+\epsilon_I}^{M+\epsilon_I} \frac{Y_m}{f_d} \left[\frac{\cos(\pi(f/f_d - m - \epsilon_F))}{(f/f_d - m - \epsilon_F)} - \frac{\operatorname{sinc}(f/f_d - m - \epsilon_F)}{(f/f_d - m - \epsilon_F)}\right]_{f=(k+\epsilon_F)f_d}$$

$$= \frac{1}{f_d} \sum_{\substack{m=-M+\epsilon_I \\ m\neq k}}^{M+\epsilon_I} Y_m \frac{(-1)^{k-m}}{k-m}. \quad (23)$$

We may simplify this by only taking the terms corresponding to $m = k \pm 1$, resulting in

$$\frac{\partial}{\partial \epsilon_F} Y_k \simeq \frac{1}{f_d}(Y_{k+1} - Y_{k-1}), \quad k = -M', -M'+1, \cdots, M'. \quad (24)$$

Hence, the additional DFT block needed to compute $\partial Y_k/\partial \epsilon_F$ in (21) may be replaced with a simple subtracter as shown in Fig. 2, dramatically reducing the implementation complexity. We refer to this simplified algorithm as *Scheme B*[2].

IV. LINEAR LOOP ANALYSIS

Let $e^A(\epsilon_F)$ and $e^B(\epsilon_F)$ denote the frequency error generated by Schemes A and B, respectively. Each FED output can be decomposed into its statistical mean and a zero mean disturbance called the *loop noise* [14] as follows:

$$e^A(\epsilon_F) = E\{e^A(\epsilon_F)\} + v_A(\epsilon_F)$$
$$e^B(\epsilon_F) = E\{e^B(\epsilon_F)\} + v_B(\epsilon_F), \quad (25)$$

where $v_A(\epsilon_F)$ and $v_B(\epsilon_F)$ denote the loop noises for Schemes A and B, respectively. Assuming that the DFT length N is large enough, the statistical means of the frequency error signals for Schemes A and B are derived in Appendix C as follows:

$$E\{e^A(\epsilon_F)\} \simeq \rho_1 \frac{2\pi}{3} \sin(2\pi\epsilon_F)$$
$$E\{e^B(\epsilon_F)\} \simeq \rho_1 \frac{4}{\pi} \sin(2\pi\epsilon_F). \quad (26)$$

Fig. 3 shows the S-curves for Schemes A and B along with computer simulation results for QPSK and 64-QAM constellations

[2]Even though Scheme B is a simplified version of Scheme A, the steady-state frequency error variance of Scheme B can be made smaller than that of Scheme A at high signal-to-noise ratio (SNR) for QPSK subcarrier modulation by setting $Y_{M'+1} = Y_{-M'-1} = 0$. See Section V and Appendix D for details.

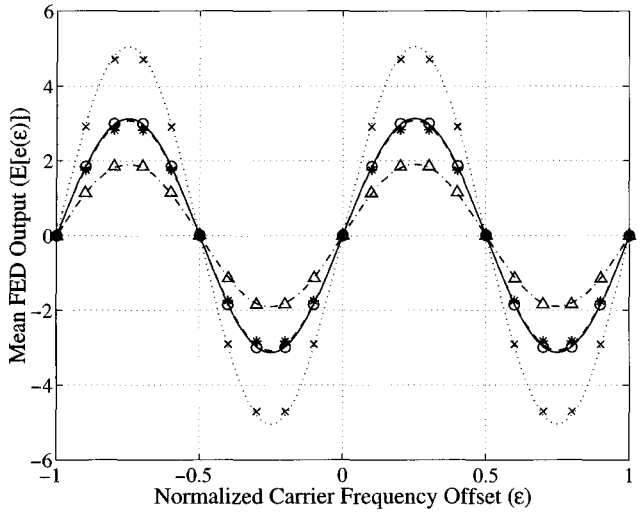

Fig. 3. S-curves for Schemes A and B assuming $E[|X_k|^2] = 1$ and $E[|H_k|^2] = 1$. Lines indicate analytical results and markers indicate computer simulation results. ($\cdots$ and $\times$: Scheme A, QPSK. — and $\circ$: Scheme A, 64-QAM. - - - and $*$: Scheme B, QPSK. - · - and $\triangle$: Scheme B, 64-QAM.)

with $E\{|X_k|^2\}$ and $E\{|H_k|^2\}$ normalized to unity. It is seen that the analytical results of (26) are in close agreement with the simulation results.

In order to analyze the steady-state behavior of tracking loop employing the proposed FEDs, we assume that $|\epsilon_F|$ is small enough so that $E\{e^A(\epsilon_F)\}$ and $E\{e^B(\epsilon_F)\}$ in (25) can safely be approximated as $E\{e^A(\epsilon_F)\} \simeq \kappa_A \epsilon_F$ and $E\{e^B(\epsilon_F)\} \simeq \kappa_B \epsilon_F$ where the FED gains κ_A and κ_B are computed from (26) as

$$\begin{aligned} \kappa_A &\triangleq \left[\frac{\partial}{\partial \epsilon_F} E\left\{e^A(\epsilon_F)\right\}\right]_{\epsilon_F=0} = \frac{4\pi^2}{3}\rho_1 \\ \kappa_B &\triangleq \left[\frac{\partial}{\partial \epsilon_F} E\left\{e^B(\epsilon_F)\right\}\right]_{\epsilon_F=0} = 8\rho_1. \end{aligned} \quad (27)$$

Furthermore, for the convenience of analysis, we approximate $v_A(\epsilon_F)$ and $v_B(\epsilon_F)$ in (25) as $v_A(\epsilon_F) \simeq v_A(0)$ and $v_B(\epsilon_F) \simeq v_B(0)$ for $|\epsilon_F| \ll 1$. By using the linearized equivalent model [14], we may then approximate (25) as

$$\begin{aligned} e^A(\epsilon_F) &\simeq \kappa_A\left(\epsilon_F + v'_A\right) \\ e^B(\epsilon_F) &\simeq \kappa_B\left(\epsilon_F + v'_B\right), \end{aligned} \quad (28)$$

where the normalized loop noises are given as $v'_A \triangleq v_A(0)/\kappa_A$ and $v'_B \triangleq v_B(0)/\kappa_B$. Then, the variance of v'_A is derived in Appendix D as

$$\sigma_A^2 = \frac{9}{2\pi^4 \rho_1^2 (2M'+1)} \sum_{i=0}^{4} \frac{v_i^A}{\gamma^i}, \quad (29)$$

where $\gamma \triangleq \sigma_s^2/\sigma_n^2$ denotes the average SNR of a subcarrier and $v_0^A = \eta_{6,2}^A - \zeta_{4,4}^A$, $v_1^A = \sigma_s^2(\eta_{6,0}^A + 9\eta_{4,2}^A - 8\zeta_{4,2}^A)$, $v_2^A = (\sigma_s^2)^2(9\eta_{4,0}^A - 4\zeta_{4,0}^A + 18\eta_{2,2}^A - 16\zeta_{2,2}^A)$, $v_3^A = (\sigma_s^2)^3(24\eta_{2,0}^A - 16\zeta_{2,0}^A)$, and $v_4^A = 2(\sigma_s^2)^4$. Here, $\eta_{n,m}^A$ and $\zeta_{n,m}^A$ are given as

$$\begin{aligned} \eta_{n,m}^A &= \frac{\mu_{n,m}^X}{2M'+1} \sum_{\substack{i=-M' \\ i\neq j}}^{M'} \sum_{j=-M+\epsilon_I}^{M+\epsilon_I} \frac{E\{|H_i|^n |H_j|^m\}}{(i-j)^2} \\ \zeta_{n,m}^A &= \frac{\mu_{n,m}^X}{2M'+1} \sum_{\substack{i=-M' \\ i\neq j}}^{M'} \sum_{j=-M'}^{M'} \frac{E\{|H_i|^n |H_j|^m\}}{(i-j)^2}, \end{aligned} \quad (30)$$

where $\mu_{n,m}^X \triangleq E\{|X_k|^n\} E\{|X_k|^m\}$. Similarly, the variance of v'_B is also derived in Appendix D as

$$\sigma_B^2 = \frac{1}{4\rho_1^2(2M'+1)} \sum_{i=0}^{4} \frac{v_i^B}{\gamma^i}, \quad (31)$$

where $v_0^B = \eta_{6,2}^B - \eta_{4,4}^B$, $v_1^B = \sigma_s^2(\eta_{6,0}^B + \eta_{4,2}^B)$, $v_2^B = (\sigma_s^2)^2(5\eta_{4,0}^B + 2\eta_{2,2}^B)$, $v_3^B = 8(\sigma_s^2)^3\eta_{2,0}^B$, and $v_4^B = 2(\sigma_s^2)^4$ with

$$\begin{aligned} \eta_{n,m}^B &= \mu_{n,m}^X E\{|H_k|^n |H_{k+1}|^m\} \\ &\simeq \mu_{n,m}^X E\left\{|H_k|^{n+m}\right\}. \end{aligned} \quad (32)$$

Since the normalized loop noises are independent among OFDM symbols, the steady-state frequency error variances for Schemes A and B are given as [15]

$$\begin{aligned} \sigma_{ss,A}^2 &= 2B_L\sigma_A^2 \\ \sigma_{ss,B}^2 &= 2B_L\sigma_B^2, \end{aligned} \quad (33)$$

where B_L is the one-sided loop bandwidth of the overall tracking loop normalized to the OFDM symbol rate $1/T$.

V. NUMERICAL RESULTS

For the numerical results presented in this section, we assume $N = 2048$, $M = 852$, $N_g = 64$, $T_s = 7/64$ μs [2], and $\epsilon_I = 100$. Then, we have $\epsilon_{GB} = 171$ and $M' = 681$.

In Figs. 4 and 5, we evaluate the steady-state performance of the proposed algorithms under AWGN and frequency selective multipath channel models. For comparison purposes, the steady-state performance of tracking loop employing van de Beek's frequency estimator [10] assuming perfect symbol timing estimation is also included. Fig. 4 shows the steady-state frequency error variance versus the average SNR, γ under AWGN channel when the normalized loop bandwidth was chosen to be $B_L = 10^{-2}$. First, we observe that the analytical results obtained using (33) fit extremely well to the simulation results for both QPSK and 64-QAM constellations. In most cases, given a constellation, the frequency error variance of Scheme B is slightly larger than that of Scheme A since Scheme B is a simple approximation of Scheme A. However, the frequency error variance of Scheme B for QPSK can be made to decrease steadily with increasing γ by adopting the condition that $Y_{M'+1} = Y_{-M'-1} = 0$ as mentioned in Appendix D. We also observe that the proposed algorithms provide considerably high error floors at high SNRs for 64-QAM. This is mainly due to large self-interference resulting from the amplitude variation

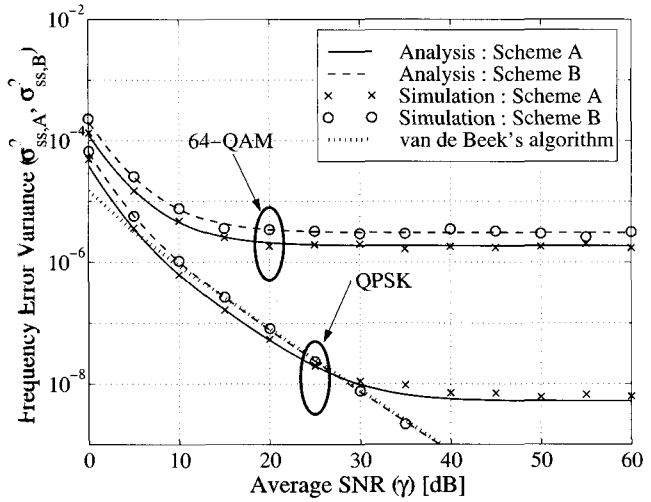

Fig 4. Steady-state frequency error variance vs. average SNR in AWGN channel. $N = 2048$, $M = 852$, $M' = 681$, $\epsilon_{GB} = 171$, $\epsilon_I = 100$, and $B_L = 10^{-2}$.

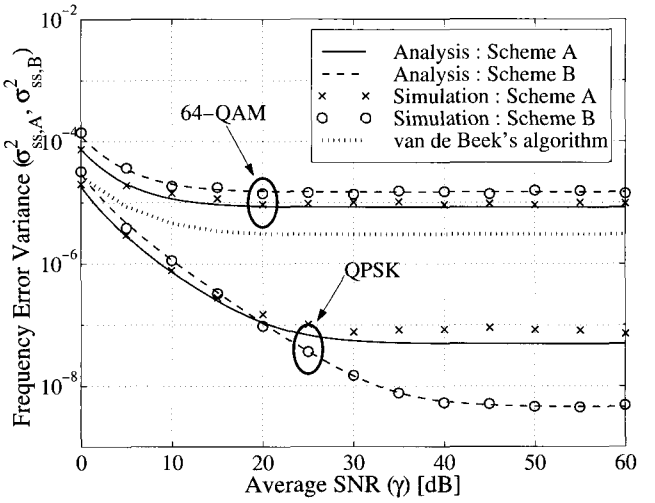

Fig. 5. Steady-state frequency error variance vs. average SNR in the assumed frequency selective multipath channel. $N = 2048$, $M = 852$, $M' = 681$, $\epsilon_{GB} = 171$, $\epsilon_I = 100$, and $B_L = 10^{-2}$.

of data symbols with high-order constellation. Finally, it is seen that the proposed algorithms achieve similar performance for QPSK but worse performance for 64-QAM when compared to van de Beek's frequency estimator. Note that the performance of van de Beek's frequency estimator is insensitive to constellation since the estimator is based on the cyclic prefix. Hence, as the constellation size increases, van de Beek's frequency estimator offers better steady-state performance than the proposed algorithms in AWGN channel.

Fig. 5 shows the steady-state frequency error variance versus γ under a frequency selective multipath channel model with the multipath profile tabulated in Table I [2]. As with Fig. 4, the normalized loop bandwidth was chosen to be $B_L = 10^{-2}$. Again, we observe that the analytical results fit quite well to the simulation results. Unlike in the case of the AWGN channel, the proposed algorithms offer significantly better steady-state performance for QPSK than van de Beek's frequency estimator. For example, the frequency error variance of Scheme A is two orders smaller than that of van de Beek's frequency estimation algorithm for $\gamma > 30$ dB and the frequency error variance of Scheme B is three orders smaller than that of van de Beek's frequency estimation algorithm for $\gamma > 40$ dB. Furthermore, it is observed from Figs. 4 and 5 that the steady-state performance degradation of the proposed algorithms due to multipath channel distortion is less severe than that of van de Beek's frequency estimation algorithm. This is because unlike van de Beek's frequency estimator, the proposed algorithms are not affected by ISI from previously transmitted OFDM symbols. Note also that the proposed algorithms operate independent of the phase of data symbol and thus the performance obtainable with general PSK is the same as that achieved with QPSK. For 64-QAM, it is seen from Figs. 4 and 5 that the steady-state performance is robust to channel dispersion but is rather poor due to the self-interference.

We now investigate the range of loop bandwidth required to satisfy given steady-state and pull-in performance requirements for the proposed algorithms under the assumed multipath channel model. The average SNR adopted in Figs. 6 and 7 was set to be $\gamma = 5.4$ dB for QPSK and $\gamma = 16$ dB for 64-QAM[3]. Fig. 6 shows a plot of the steady-state frequency error variance as a function of the loop bandwidth B_L. Again, we observe that the analytical results are in close agreement with the simulation results for the wide range of B_L considered. Since the frequency error variance increases linearly with B_L, maximum allowable frequency error variance places an upper bound of B_L. For example, say that we desire the standard deviation of the steady-

Table 1. Attenuation, delay, and phase values for the assumed frequency selective multipath channel.

i	$\lvert h_i \rvert$	$\tau_i[\mu s]$	$\angle h_i$[rad]
0	0.225894	0.0	2.128544
1	0.150340	0.069673	3.952093
2	0.051534	0.079949	1.093586
3	0.149723	0.120324	3.462951
4	0.170996	0.130069	1.099463
5	0.295723	0.356065	5.928383
6	0.407163	0.444767	5.864470
7	0.258782	0.529012	3.758058
8	0.221155	0.566629	3.334290
9	0.262909	0.774948	0.628578
10	0.240140	0.850567	3.664773
11	0.057662	0.929136	4.855121
12	0.061831	0.942702	5.430202
13	0.259730	1.29479	0.393889
14	0.116587	1.30744	2.833799
15	0.400967	1.86169	0.154459
16	0.303585	2.67789	2.215894
17	0.350825	3.15499	3.053023
18	0.185074	3.25098	5.775198
19	0.176809	5.34821	3.419109

[3]These values of γ are the required SNRs for non-hierarchical transmission to achieve a bit error rate of 2×10^{-4} after inner Viterbi decoding. This corresponds to quasi-error free condition after outer Reed-Solomon decoding [2].

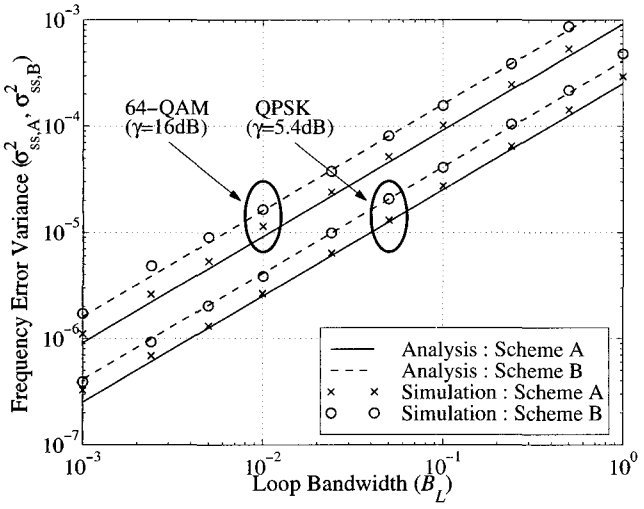

Fig. 6. Steady-state frequency error variance vs. loop bandwidth over the assumed frequency selective multipath channel for $\gamma = 5.4$ dB for QPSK and $\gamma = 16$ dB for 64-QAM. $N = 2048$, $M = 852$, $M' = 681$, $\epsilon_{GB} = 171$, and $\epsilon_I = 100$.

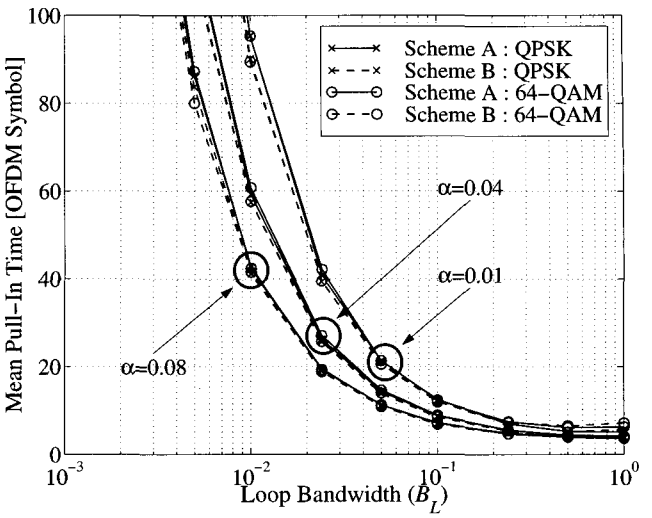

Fig. 7. Mean pull-in time vs. loop bandwidth in a first-order loop over the assumed frequency selective multipath channel for $\gamma = 5.4$ dB for QPSK and $\gamma = 16$ dB for 64-QAM. $N = 2048$, $M = 852$, $M' = 681$, $\epsilon_{GB} = 171$, and $\epsilon_I = 100$.

state frequency error to be less than 1 % of the subcarrier spacing[4] at $\gamma = 5.4$ dB for QPSK with Scheme B. Then, the results indicate that B_L should be chosen to be less than 2.4×10^{-1}.

Next, in order to investigate the pull-in performance, we define $e[m] \triangleq \epsilon_F - \hat{\epsilon}_F[m]$ to be the residual frequency error at the mth OFDM symbol time where ϵ_F is the initial fractional carrier frequency offset and $\hat{\epsilon}_F[m]$ is the estimated carrier frequency offset with the initial value of zero. We define the frequency pull-in condition as the case when the frequency error satisfies $|e[m]| \leq \alpha$ and the pull-in time as the smallest time at which the frequency pull-in condition is satisfied. Fig. 7 shows a plot of the mean pull-in time as a function of B_L for a first-order loop with $\alpha = 0.01, 0.04$, and 0.08 when ϵ_F is assumed to be uniformly distributed in $[-1/2, 1/2)$. Since the mean pull-in time decreases as B_L increases, maximum allowable mean pull-in time places a lower bound on B_L. For example, say that we desire the mean pull-in time to be less than 25 OFDM symbols at $\gamma = 5.4$ dB for QPSK with Scheme B with $\alpha = 0.04$. Then, the results indicate that B_L should be chosen to be larger than 2.4×10^{-2}. This, together with the upper bound obtained for the example in Fig. 6, results in the usable range of B_L as $2.4 \times 10^{-2} \leq B_L \leq 2.4 \times 10^{-1}$.

Finally, we investigate the influence of ISI due to symbol timing offsets on the steady-state performance of the proposed algorithms[5]. We assume that $y(t)$ in (4) is sampled at $t = mT + nT_s + \theta T_s$, $n = 0, 1, \cdots, N-1$, to yield the N-point DFT input sequence of the mth OFDM symbol where θ denotes the symbol timing offset normalized to T_s. Figs. 8(a) and 8(b) show the steady-state frequency error variances as a function of θ for QPSK and 64-QAM, respectively, when $B_L = 0.01, 0.025, 0.05$, and 0.1. As with Figs. 6 and 7, the average SNR was chosen to be $\gamma = 5.4$ dB for QPSK and $\gamma = 16$ dB for 64-QAM. We observe that the frequency error variance increases as θ increases, but the increase in the frequency error variance is not significant for the range of θ considered. This implies that the decrease in the average SNR due to the ISI-induced ICI caused by symbol timing offsets is not severe, and thus the proposed algorithms are insensitive to symbol timing offsets, requiring only a crude symbol timing recovery.

VI. CONCLUSIONS

In this paper, an NDA nonlinear spectral-line carrier frequency synchronization algorithm and its hardware efficient modification were proposed for OFDM receivers. Analytical expressions were derived for the steady-state frequency error variances and their accuracy was verified via computer simulations for QPSK and 64-QAM subcarrier modulations under AWGN and frequency selective multipath channels. For QPSK, the proposed algorithms achieve significantly better and reliable steady-state performance over an assumed multipath channel model compared to van de Beek's frequency estimator. For 64-QAM, however, the proposed algorithms suffer from large performance degradation at high SNRs due to self-interference. Hence, operating independent of the phase of transmitted symbol, the proposed algorithms may be suitable for PSK or low-order QAM subcarrier modulations. Analytical and simulation results were also provided for the design of proper loop bandwidths in order to achieve a desired steady-state and pull-in performance.

APPENDIX A
SIMPLIFICATION OF $E\{|\tilde{Y}_k|^{2q}\}$ IN (13)

[4]The required carrier frequency accuracy may be chosen so as to satisfy a given transmission quality such as bit-error-rate.

[5]In OFDM receivers, symbol timing offsets may cause linear phase rotation of the receiver DFT output and ISI-induced ICI [16]. However, the proposed algorithms based on the absolute moments of the DFT outputs are not affected by the phase rotation of the DFT outputs, and thus, we only consider the effect of ISI-induced ICI.

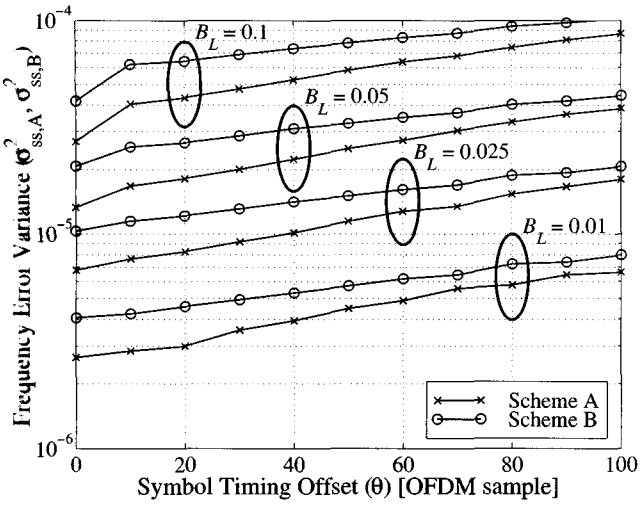

(a)

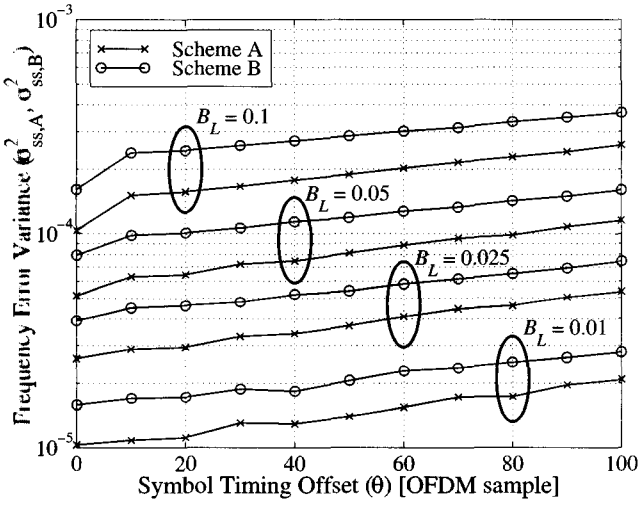

(b)

Fig. 8. Frequency error variance vs. symbol timing offset over the assumed frequency selective multipath channel for $\gamma = 5.4$ dB for QPSK and $\gamma = 16$ dB for 64-QAM. $N = 2048$, $M = 852$, $M' = 681$, $GB = 171$, and $\epsilon_I = 100$: (a) QPSK, (b) 64-QAM.

Assuming $H_{l-\epsilon_I} = 1$ for all l, $E\{|\tilde{Y}_k|^{2q}\}$ in (13) can be expanded as

$$E\left\{|\tilde{Y}_k|^{2q}\right\} = E\left\{\left|\sum_{l=-N/2}^{N/2-1} X_{l-\epsilon_I} e^{j\phi}\Psi_l^k\right|^{2q}\right\}$$
$$= \sum_{l_1=-N/2}^{N/2-1}\sum_{l_2=-N/2}^{N/2-1}\cdots\sum_{l_{2q}=-N/2}^{N/2-1}\prod_{j=1}^{q}\Psi_{l_{2j-1}}^k\left(\Psi_{l_{2j}}^k\right)^*$$
$$\times E\left\{\prod_{j=1}^{q} X_{l_{2j-1}-\epsilon_I}X_{l_{2j}-\epsilon_I}^*\right\}. \quad \text{(A.34)}$$

Given a set of summation indices $l_1, l_2, \cdots, l_{2q}$, we define $L^o \triangleq \{l_1, l_3, \cdots, l_{2q-1}\}$ and $L^e \triangleq \{l_2, l_4, \cdots, l_{2q}\}$. Furthermore, we set $\tilde{L}_m^o \triangleq \{l_{m,1}^o, l_{m,2}^o, \cdots, l_{m,m}^o\}$ with $l_{m,j}^o$ being the jth element of the m $(1 \le m \le q)$ distinct elements within L^o and $D_m^o \triangleq \{d_{m,1}^o, d_{m,2}^o, \cdots, d_{m,m}^o\}$ with $d_{m,j}^o$ being the number of occurrences of $l_{m,j}^o$ within L^o satisfying $1 \le d_{m,1}^o \le d_{m,2}^o \le \cdots \le d_{m,m}^o \le q$. Similarly, we set $\tilde{L}_n^e \triangleq \{l_{n,1}^e, l_{n,2}^e, \cdots, l_{n,n}^e\}$ with $l_{n,j}^e$ being the jth element of the n $(1 \le n \le q)$ distinct elements within L^e and $D_n^e \triangleq \{d_{n,1}^e, d_{n,2}^e, \cdots, d_{n,n}^e\}$ with $d_{n,j}^e$ being the number of occurrences of $l_{n,j}^e$ within L^e satisfying $1 \le d_{n,1}^e \le d_{n,2}^e \le \cdots \le d_{n,n}^e \le q$. Note that $\sum_{j=1}^m d_{m,j}^o = \sum_{j=1}^n d_{n,j}^e = q$. Since the transmitted data $X_{l-\epsilon_I}$ are assumed to be statistically i.i.d. with zero mean for all subcarriers, the term $E\{\prod_{j=1}^q X_{l_{2j-1}-\epsilon_I}X_{l_{2j}-\epsilon_I}^*\}$ in (A.34) can then be computed to be

$$E\left\{\prod_{j=1}^{q} X_{l_{2j-1}-\epsilon_I}X_{l_{2j}-\epsilon_I}^*\right\}$$
$$= \begin{cases} \prod_{j=1}^m E\left\{\left|X_{l_j-\epsilon_I}\right|^{2d_{m,j}}\right\}, \\ \qquad m = n,\ \tilde{L}_e^m = \tilde{L}_o^n \text{ and } D_e^m = D_o^n \\ 0, \qquad \text{otherwise,} \end{cases} \quad \text{(A.35)}$$

where $d_{m,j} = d_{m,j}^e$ for $j = 1, 2, \cdots, m$. Then, $E\{|\tilde{Y}_k|^{2q}\}$ can be given as

$$E\left\{|\tilde{Y}_k|^{2q}\right\} = \sum_{i=1}^{q}\sum_{\mathbf{d_i}\in\mathcal{D}_i} a(\mathbf{d_i})\sum_{\mathbf{l_i}}\prod_{j=1}^{i} E\left\{\left|X_{l_j-\epsilon_I}\right|^{2d_{i,j}}\right\}$$
$$\times\prod_{j=1}^{i}\left|\Psi_{l_j}^k\right|^{2d_{i,j}}, \quad \text{(A.36)}$$

where $\mathcal{D}_\mathbf{i} = \{\mathbf{d_i} = (d_{i,1}, d_{i,2}, \cdots, d_{i,i}) \mid \sum_{j=1}^i d_{i,j} = q, d_{i,j} \in \{1, 2, 3, \cdots, q\}, d_{i,1} \le d_{i,2} \le \cdots \le d_{i,i}\}$ and

$$\sum_{\mathbf{l_i}} \triangleq \sum_{l_1=-N/2}^{N/2-1}\sum_{\substack{l_2=-N/2\\ l_2\neq l_1}}^{N/2-1}\cdots\sum_{\substack{l_i=-N/2\\ l_i\neq l_1,\cdots,l_i\neq l_{i-1}}}^{N/2-1}. \quad \text{(A.37)}$$

Also, the term $a(\mathbf{d_i})$ denoting the number of the terms in (A.34) satisfying $\tilde{L}_e^i = \tilde{L}_o^i$ given $D_e^i = D_o^i = \mathbf{d_i}$ can be computed as

$$a(\mathbf{d_i}) = \left(\frac{q!}{d_{i,1}!d_{i,2}!\cdots d_{i,i}!}\right)^2 \frac{1}{e_{i,1}!e_{i,2}!\cdots e_{i,m_i}!}, \quad \text{(A.38)}$$

where $e_{i,m}$, $m = 1, 2, \cdots, m_i$ $(m_i \le i)$ is the number of occurrences of the m_i distinct components in $\mathbf{d_i} = (d_{i,1}, d_{i,2}, \cdots, d_{i,i})$. Since $X_{l-\epsilon_I}$ are statistically i.i.d., (A.36) can be simplified as

$$E\left\{|\tilde{Y}_k|^{2q}\right\} = \sum_{i=1}^{q}\sum_{\mathbf{d_i}\in\mathcal{D}_i} a(\mathbf{d_i})\prod_{j=1}^{i} E\left\{|X_k|^{2d_{i,j}}\right\}$$
$$\times\sum_{\mathbf{l_i}}\prod_{j=1}^{i}\left|\Psi_{l_j}^k\right|^{2d_{i,j}}. \quad \text{(A.39)}$$

For positive integers x and y, we have

$$\sum_{\substack{l_1=-N/2\\ l_1\neq l_2}}^{N/2-1}\sum_{l_2=-N/2}^{N/2-1}|\Psi_{l_1}^k|^{2x}|\Psi_{l_2}^k|^{2y}$$

$$= \Gamma_x(\epsilon_F)\Gamma_y(\epsilon_F) - \Gamma_{x+y}(\epsilon_F), \quad \text{(A.40)}$$

where $\Gamma_x(\epsilon_F)$ is defined as (18) and shown in Appendix B to be

$$\Gamma_x(\epsilon_F) = \sum_{m=0}^{x-1} c_m^x \cos(2\pi m\epsilon_F), \quad \text{(A.41)}$$

yielding

$$\Gamma_x(\epsilon_F)\Gamma_y(\epsilon_F) = \sum_{m_1=0}^{x-1}\sum_{m_2=0}^{y-1} \frac{c_{m_1}^x c_{m_2}^y}{2} \times \left(\cos(2\pi(m_1+m_2)\epsilon_F) + \cos(2\pi(m_1-m_2)\epsilon_F)\right). \quad \text{(A.42)}$$

Thus, it follows from (A.41) and (A.42) that (A.40) can be expressed as a linear combination of $\cos(2\pi m\epsilon_F)$, $m = \min\{-(x-1), -(y-1)\}, \min\{-(x-1), -(y-1)\}+1, \cdots, (x+y-1)$. Hence, by repeated application of (A.40) to (A.39), we can easily check that $E\{|\tilde{Y}_k|^{2q}\}$ is a linear combination of $\cos(2\pi m\epsilon_F)$, $m = 0, \pm 1, \pm 2, \cdots, \pm(q-1)$.

APPENDIX B
COSINE EXPANSION OF $\Gamma_q(\epsilon_F)$

In this appendix, we compute the cosine expansion of $\Gamma_q(\epsilon_F)$ defined as (18). Substituting (8) into (18) yields

$$\Gamma_q(\epsilon_F) = \frac{1}{N^{2q}} \sum_{\mathbf{n_{2q}}\in\mathcal{N}} \sum_{l=-N/2}^{N/2-1} e^{j2\pi(l-k+\epsilon_F)f(\mathbf{n_{2q}})/\mathbf{N}}, \quad \text{(B.43)}$$

where $\mathcal{N} = \{\mathbf{n_{2q}} = (n_1, n_2, \cdots, n_{2q}) \mid n_1, n_2, \cdots, n_{2q} \in \{0, 1, 2, \cdots, N-1\}\}$ and $f(\mathbf{n_{2q}}) = (n_1 - n_2) + \cdots + (n_{2q-1} - n_{2q})$. Note that $f(\mathbf{n_{2q}})$ is an integer value between $-(N-1)q$ and $(N-1)q$. For some integer r, we have

$$\frac{1}{N}\sum_{l=-N/2}^{N/2-1} \exp\left(\frac{j2\pi rl}{N}\right) = \begin{cases} 1, & r = mN \\ 0, & \text{otherwise,} \end{cases} \quad \text{(B.44)}$$

where m is an integer. Thus, (B.43) is nonzero only if $f(\mathbf{n_{2q}}) = mN$ for some integer m satisfying $|m| \le q-1$ and reduces to

$$\Gamma_q(\epsilon_F) = \sum_{m=-q+1}^{q-1} z_m^q \exp(j2\pi m\epsilon_F), \quad \text{(B.45)}$$

where z_m^q is the number of elements in $\mathcal{Z} = \{\mathbf{z_{2q}} = (z_1, z_2, \cdots, z_{2q}) \mid \mathbf{z_{2q}} \in \mathcal{N}, f(\mathbf{z_{2q}}) = mN\}$ divided by N^{2q-1}. Since $z_{-m}^q = z_m^q$, (B.45) can alternatively be expressed as

$$\Gamma_q(\epsilon_F) = \sum_{m=0}^{q-1} c_m^q \cos(2\pi m\epsilon_F), \quad \text{(B.46)}$$

where $c_0^q = z_0^q$ and $c_m^q = 2z_m^q$ for $m \neq 0$. For the case of $q = 1$ and $q = 2$, the z_m^q's can easily be computed, yielding

$$\Gamma_1(\epsilon_F) = 1 \quad \text{(B.47)}$$
$$\Gamma_2(\epsilon_F) = \frac{1}{3}\left(1 - \frac{1}{N^2}\right)\cos(2\pi\epsilon_F) + \frac{2}{3}\left(1 + \frac{1}{2N^2}\right).$$

APPENDIX C
MEANS OF THE FREQUENCY ERROR SIGNALS

In this appendix, the statistical means of the frequency error signals for Schemes A and B in (25) are computed. From (20), the stochastic update frequency error signal for Scheme A is given by

$$e^A(\epsilon_F) = \frac{1}{2M'+1}\sum_{k=-M'}^{M'} \frac{\partial}{\partial\epsilon_F}|Y_k|^4. \quad \text{(C.48)}$$

The mean of $e^A(\epsilon_F)$ is then written as

$$E\left\{e^A(\epsilon_F)\right\} = \frac{1}{2M'+1}\sum_{k=-M'}^{M'} \frac{\partial}{\partial\epsilon_F} E\left\{|Y_k|^4\right\}. \quad \text{(C.49)}$$

Substituting $\partial E\{|Y_k|^4\}/\partial\epsilon_F$ obtained by differentiating (17) with respect to ϵ_F into (C.49) yields

$$E\left\{e^A(\epsilon_F)\right\} \simeq \rho_1\frac{2\pi}{3}\left(1 - \frac{1}{N^2}\right)\sin(2\pi\epsilon_F). \quad \text{(C.50)}$$

For sufficiently large N, (C.50) can further be approximated as

$$E\left\{e^A(\epsilon_F)\right\} \simeq \rho_1\frac{2\pi}{3}\sin(2\pi\epsilon_F). \quad \text{(C.51)}$$

Next, it follows from (20) and (24) that the frequency error signal for Scheme B is given as

$$e^B(\epsilon_F) = \sum_{k=-M'}^{M'} \frac{4|Y_k|^2 \operatorname{Re}\left[Y_k^*(Y_{k+1} - Y_{k-1})\right]}{2M'+1}. \quad \text{(C.52)}$$

By substituting (12) into (C.52) and taking the expectation operation of the resulting expression, we obtain the mean of (C.52) as

$$E\left\{e^B(\epsilon_F)\right\} = -4\rho_1\alpha_1(\epsilon_F) + 4\rho_2\alpha_2(\epsilon_F), \quad \text{(C.53)}$$

where $\alpha_1(\epsilon_F)$ and $\alpha_2(\epsilon_F)$ are given as

$$\alpha_1(\epsilon_F) = \operatorname{Re}\left[\sum_{l=-N/2}^{N/2-1} \left|\Psi_l^k\right|^2 \left(\Psi_l^k\right)^* \left(\Psi_l^{k+1} - \Psi_l^{k-1}\right)\right]$$
$$\alpha_2(\epsilon_F) = \sum_{l_1=-N/2}^{N/2-1} \left|\Psi_{l_1}^k\right|^2 \times \operatorname{Re}\left[\sum_{l_2=-N/2}^{N/2-1} \left(\Psi_{l_2}^k\right)^* \left(\Psi_{l_2}^{k+1} - \Psi_{l_2}^{k-1}\right)\right]. \quad \text{(C.54)}$$

From (8) and (B.44), $\alpha_1(\epsilon_F)$ and $\alpha_2(\epsilon_F)$ can further be reduced to

$$\alpha_1(\epsilon_F) = \sum_{m=-1}^{1} \frac{\operatorname{Re}\left[-j2\exp(j2\pi m\epsilon_F)\right]}{N^3} \times \sum_{\substack{n_1=0\\ n_1+n_2=n_3+n_4+mN}}^{N-1}\sum_{n_2=0}^{N-1}\sum_{n_3=0}^{N-1}\sum_{n_4=0}^{N-1} \sin\left(\frac{2\pi n_1}{N}\right)$$

$$
\begin{aligned}
&= \sin(2\pi\epsilon_F)\sum_{n=1}^{N-1}\sin\left(\frac{2\pi n}{N}\right)\\
&\quad\times\left(\frac{n(n+1)}{2N^3}-\frac{(N-n-1)(N-n)}{2N^3}\right)\\
&\simeq -\frac{1}{\pi}\sin(2\pi\epsilon_F), \qquad \text{for } N\gg 1\\
\alpha_2(\epsilon_F) &= \mathrm{Re}\left[\frac{1}{N}\sum_{n=0}^{N-1}\left(e^{-j2\pi n/N}-e^{j2\pi n/N}\right)\right]\\
&= 0. \qquad \text{(C.55)}
\end{aligned}
$$

Hence, (C.53) reduces to

$$
E\left\{e^B(\epsilon_F)\right\} \simeq \rho_1\frac{4}{\pi}\sin(2\pi\epsilon_F). \qquad \text{(C.56)}
$$

APPENDIX D
VARIANCES OF THE FREQUENCY ERROR SIGNALS

In this appendix, we derive the variances of the normalized loop noises v'_A and v'_B in (28). The second moment of the frequency error signal of (20) is given as

$$
\begin{aligned}
&E\left\{|e(\epsilon_F)|^2\right\}\\
&= E\left\{\left|\frac{4}{2M'+1}\sum_{k=-M'}^{M'}|Y_k|^2\,\mathrm{Re}\left[Y_k^*\frac{\partial}{\partial\epsilon_F}Y_k\right]\right|^2\right\}\\
&= \frac{16}{(2M'+1)^2}\left(\beta_1(\epsilon_F)+\beta_2(\epsilon_F)\right), \qquad \text{(D.57)}
\end{aligned}
$$

where $\beta_1(\epsilon_F)$ and $\beta_2(\epsilon_F)$ are written as

$$
\begin{aligned}
\beta_1(\epsilon_F) &= \sum_{k=-M'}^{M'}E\left\{|Y_k|^4\mathrm{Re}^2\left[Y_k^*\frac{\partial}{\partial\epsilon_F}Y_k\right]\right\}\\
&= \frac{1}{2}\sum_{k=-M'}^{M'}E\left\{|Y_k|^4\left|Y_k^*\frac{\partial}{\partial\epsilon_F}Y_k\right|^2\right\} \qquad \text{(D.58)}\\
\beta_2(\epsilon_F) &= \sum_{\substack{k_1=-M'\\k_1\neq k_2}}^{M'}\sum_{k_2=-M'}^{M'}E\left\{|Y_{k_1}|^2|Y_{k_2}|^2\right.\\
&\quad\left.\times\,\mathrm{Re}\left[Y_{k_1}^*\frac{\partial}{\partial\epsilon_F}Y_{k_1}\right]\mathrm{Re}\left[Y_{k_2}^*\frac{\partial}{\partial\epsilon_F}Y_{k_2}\right]\right\}\\
&= \frac{1}{2}\sum_{\substack{k_1=-M'\\k_1\neq k_2}}^{M'}\sum_{k_2=-M'}^{M'}E\left\{|Y_{k_1}|^2|Y_{k_2}|^2\right.\\
&\quad\left.\times\,\mathrm{Re}\left[Y_{k_1}^*\frac{\partial}{\partial\epsilon_F}Y_{k_2}\cdot Y_{k_2}^*\frac{\partial}{\partial\epsilon_F}Y_{k_1}\right]\right\}. \qquad \text{(D.59)}
\end{aligned}
$$

Here, the last steps in (D.58) and (D.59) are, respectively, obtained by using the following relations:

$$
\begin{aligned}
\mathrm{Re}^2[x] &= \frac{1}{2}|x|^2+\frac{1}{2}\mathrm{Re}\left[x^2\right]\\
\mathrm{Re}[x]\,\mathrm{Re}[y] &= \frac{1}{2}\mathrm{Re}[xy]+\frac{1}{2}\mathrm{Re}\left[xy^*\right]. \qquad \text{(D.60)}
\end{aligned}
$$

By substituting (23) into (D.58) and (D.59) and then substituting the resulting expressions into (D.57), we obtain the second moment of the frequency error signal for Scheme A, resulting in

$$
\begin{aligned}
E\left\{|e^A(\epsilon_F)|^2\right\} &= \frac{8}{(2M'+1)^2}\sum_{k=-M'}^{M'}\\
&\left(\sum_{\substack{m=-M+\epsilon_I\\m\neq k}}^{M+\epsilon_I}\frac{E\left\{|Y_k|^6|Y_m|^2\right\}}{(k-m)^2}-\sum_{\substack{m=-M'\\m\neq k}}^{M'}\frac{E\left\{|Y_k|^4|Y_m|^4\right\}}{(k-m)^2}\right). \qquad \text{(D.61)}
\end{aligned}
$$

Taking the terms with $m=k\pm 1$ in (D.61) yields the second moment of the frequency error signal for Scheme B, given as

$$
\begin{aligned}
E\left\{|e^B(\epsilon_F)|^2\right\} &= 8\sum_{k=-M'}^{M'}\\
&\frac{E\left\{|Y_k|^6\left(|Y_{k+1}|^2+|Y_{k-1}|^2\right)-|Y_k|^4\left(|Y_{k+1}|^4+|Y_{k-1}|^4\right)\right\}}{(2M'+1)^2}\\
&+\frac{8\left(E\left\{|Y_{M'}|^4|Y_{M'+1}|^4\right\}+E\left\{|Y_{-M'}|^4|Y_{-M'-1}|^4\right\}\right)}{(2M'+1)^2}. \qquad \text{(D.62)}
\end{aligned}
$$

Note that since the FED of Scheme B processes only the DFT outputs unlike that of Scheme A, the last term in (D.62) possibly resulting in an error floor of the steady-state frequency error variance at high SNRs can be eliminated by setting $Y_{M'+1}=Y_{-M'-1}=0$.

Recalling that $v'_A=v_A(0)/\kappa_A$, the variance of v'_A can be obtained by substituting (12) with $\epsilon_F=0$ into (D.61) and normalizing the resulting expression by κ_A^2. Through straight but somewhat tedious calculations, we can show that the variance of v'_A is derived as

$$
\begin{aligned}
\sigma_A^2 &\triangleq \frac{E\left\{|e^A(0)|^2\right\}}{\kappa_A^2}\\
&= \frac{9}{2\pi^4\rho_1^2(2M'+1)}\sum_{i=0}^{4}\frac{v_i^A}{\gamma^i}, \qquad \text{(D.63)}
\end{aligned}
$$

where $\gamma\triangleq\sigma_s^2/\sigma_n^2$ denotes the average SNR of a subcarrier and $v_0^A=\eta_{6,2}^A-\zeta_{4,4}^A$, $v_1^A=\sigma_s^2(\eta_{6,0}^A+9\eta_{4,2}^A-8\zeta_{4,2}^A)$, $v_2^A=(\sigma_s^2)^2(9\eta_{4,0}^A-4\zeta_{4,0}^A+18\eta_{2,2}^A-16\zeta_{2,2}^A)$, $v_3^A=(\sigma_s^2)^3(24\eta_{2,0}^A-16\zeta_{2,0}^A)$, and $v_4^A=2(\sigma_s^2)^4$. Here, $\eta_{n,m}^A$ and $\zeta_{n,m}^A$ are given as

$$
\begin{aligned}
\eta_{n,m}^A &= \frac{\mu_{n,m}^X}{2M'+1}\sum_{i=-M'}^{M'}\sum_{\substack{j=-M+\epsilon_I\\i\neq j}}^{M+\epsilon_I}\frac{E\left\{|H_i|^n|H_j|^m\right\}}{(i-j)^2} \qquad \text{(D.64)}\\
\zeta_{n,m}^A &= \frac{\mu_{n,m}^X}{2M'+1}\sum_{i=-M'}^{M'}\sum_{\substack{j=-M'\\i\neq j}}^{M'}\frac{E\left\{|H_i|^n|H_j|^m\right\}}{(i-j)^2}, \qquad \text{(D.65)}
\end{aligned}
$$

where $\mu_{n,m}^X\triangleq E\left\{|X_k|^n\right\}E\left\{|X_k|^m\right\}$. Similarly, by substituting (12) with $\epsilon_F=0$ into (D.62) and normalizing the resulting

expression by κ_B^2, we can derive the variance of v_B' as

$$\sigma_B^2 \triangleq \frac{E\left\{|e^B(0)|^2\right\}}{\kappa_B^2} = \frac{1}{4\rho_1^2(2M'+1)} \sum_{i=0}^{4} \frac{v_i^B}{\gamma^i}, \quad \text{(D.66)}$$

where $v_0^B = \eta_{6,2}^B - \eta_{4,4}^B$, $v_1^B = \sigma_s^2(\eta_{6,0}^B + \eta_{4,2}^B)$, $v_2^B = (\sigma_s^2)^2(5\eta_{4,0}^B + 2\eta_{2,2}^B)$, $v_3^B = 8(\sigma_s^2)^3\eta_{2,0}^B$, and $v_4^B = 2(\sigma_s^2)^4$ with

$$\eta_{n,m}^B = \mu_{n,m}^X E\left\{|H_k|^n |H_{k+1}|^m\right\}. \quad \text{(D.67)}$$

Since the channel response is assumed to be approximately constant among closely spaced subcarriers, (D.67) can be approximated as

$$\eta_{n,m}^B \simeq \mu_{n,m}^X E\left\{|H_k|^{n+m}\right\}. \quad \text{(D.68)}$$

REFERENCES

[1] J. A. Bingham, "Multicarrier modulation for data transmission: An idea whose time has come," *IEEE Commun. Mag.*, vol. 28, pp. 5–14, May 1990.

[2] ETSI, "Digital video broadcasting(DVB): Framing structure, channel coding and modulation for digital terrestrial television," EN 300 744, Aug. 1997.

[3] IEEE 802.11, "Supplement to standard for information technology - telecommunications and information exchange between systems - local and metropolitan area networks - specific requirements - part 11: Wireless LAN MAC and PHY specifications: High speed physical layer in the 5 GHz band," IEEE Std 802.11a, 1999.

[4] IEEE 802.11, "Draft supplement to standard for information technology - telecommunications and information exchange between systems - local and metropolitan area networks - specific requirements - part 11: Wireless LAN MAC and PHY specifications: Further higher-speed physical layer extension in the 2.4 GHz band," IEEE Std 802.11g/D3.0, July 2002.

[5] T. Pollet, M. V. Bladel, and M. Moeneclaey, "BER sensitivity of OFDM systems to carrier frequency offset and wiener phase noise," *IEEE Trans. Commun.*, vol. 43, pp. 191–193, Feb. 1995.

[6] P. H. Moose, "A technique for orthogonal frequency division multiplexing frequency offset correction," *IEEE Trans. Commun.*, vol. 42, no. 10, pp. 2908–2914, Oct. 1994.

[7] F. Daffara and O. Adami, "A new frequency detector for orthogonal multicarrier transmission techniques," in *Proc. IEEE VTC*, vol. 2, July 1995, pp. 804–809.

[8] T. M. Schmidl and D. C. Cox, "Robust frequency and timing synchronization for OFDM," *IEEE Trans. Commun.*, vol. 45, no. 12, pp. 1613–1621, Dec. 1997.

[9] M. Morelli and U. Mengali, "An improved frequency offset estimator for OFDM applications," *IEEE Trans. Commun. Lett.*, vol. 3, no. 3, pp. 75–77, Mar. 1999.

[10] J. J. van de Beek, M. Sandell, and P. O. Borjesson, "ML estimation of time and frequency offset in OFDM systems," *IEEE Trans. Signal Processing*, vol. 45, pp. 1800–1805, July 1997.

[11] M. Morelli, A. D'Andrea, and U. Mengali, "Frequency ambiguity resolution in OFDM systems," *IEEE Trans. Commun. Lett.*, vol. 4, no. 4, pp. 134–136, Apr. 2000.

[12] J. G. Proakis, *Digital Communication*, New York: McGraw-Hill, 1995.

[13] E. A. Lee and D. G. Messerschmitt, *Digital Communication*, Norwell, MA: Kluwer Academic Publishers, 1994.

[14] H. Meyr, M. Moeneclaey, and S. A. Fechtel, *Digital Communication Receivers: Synchronization, Channel Estimation, and Singal Processing*, New York: John Wiley & Sons, Inc., 1998.

[15] W. C. Lindsey and C. M. Chie, "A survey of digital phase-locked loops," *Proc. IEEE*, vol. 69, pp. 410–431, Apr. 1981.

[16] B. Yang *et al.*, "Timing recovery for OFDM transmission," *IEEE J. Select. Areas Commun.*, vol. 18, no. 11, pp. 2278–2291, Nov. 2000.

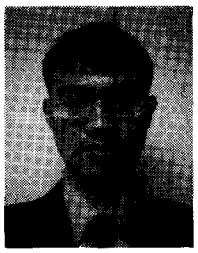

Heejin Roh was born in Seoul, Korea, on October 6, 1971. He received the B.S., M.S., and Ph.D. degrees in electronic and electrical engineering from Pohang University of Science and Technology (POSTECH), Pohang, Korea, in 1995, 1997, and 2004, respectively. He is currently with Samsung Electronics Co., Ltd., Korea, where he is engaged in the development of cdma2000 1x EV-DV modem chipsets. His current research interests include synchronization, OFDM systems, DS-CDMA systems, and turbo codes.

Kyungwhoon Cheun was born in Seoul, Korea, on December 16, 1962. He received the B.A. degree in electronics engineering from Seoul National University, Seoul, Korea, in 1985, and the M.S. and Ph.D. degrees from the University of Michigan, Ann Arbor, in 1987 and 1989, respectively, both in electrical engineering. From 1987 to 1989, he was a Research Assistant at the EECS Department at the University of Michigan, and from 1989 to 1991, he joined the Electrical Engineering Department at the University of Delaware, Newark, as an Assistant Professor. In 1991, he joined the Division of Electrical and Computer Engineering at the Pohang University of Science and Technology (POSTECH), Pohang, Korea, where he is currently a Professor. He also served as an engineering consultant to various industries in the area of mobile communications and modem design. His current research interests include turbo codes, RA codes, space-time codes, MIMO systems, UWB communications, cellular and packet radio networks, and OFDM systems.